minerals

MDPI

Article

Sr–Nd–Pb–Hf Isotopic Constraints on the Mantle Heterogeneities beneath the South Mid-Atlantic Ridge at 18–21°S

Yun Zhong [1,2], Xu Zhang [1,3,4], Zhilei Sun [1,2], Jinnan Liu [5], Wei Li [1,3,4], Yaoliang Ma [1,3,4], Weiliang Liu [1,2,*], Bin Xia [1,3,4] and Yao Guan [6]

1 School of Marine Sciences, Sun Yat-sen University, Guangzhou 510006, China; zhongy73@mail.sysu.edu.cn (Y.Z.); zhangx729@mail2.sysu.edu.cn (X.Z.); zhileisun@yeah.net (Z.S.); liwei237@mail2.sysu.edu.cn (W.L.); mayliang@mail2.sysu.edu.cn (Y.M.); xiabin08@outlook.com (B.X.)
2 The Key Laboratory of Gas Hydrate, Ministry of Natural Resources, Qingdao Institute of Marine Geology, Qingdao 266071, China
3 Guangdong University Key Laboratory of Offshore Oil Exploration and Development/Guangdong Provincial Key Laboratory of Marine Resources and Coastal Engineering, School of Marine Sciences, Sun Yat-sen University, Guangzhou 510006, China
4 Southern Laboratory of Ocean Science and Engineering (Guangdong, Zhuhai), Zhuhai 519000, China
5 Yunnan Seismological Bureau, Kunming 530100, China; liujn27@mail2.sysu.edu.cn
6 Fourth Institute of Oceanography, Ministry of Natural Resources, Beihai 536000, China; guanyao@mail2.sysu.edu.cn
* Correspondence: liuweil@mail.sysu.edu.cn

Received: 18 October 2020; Accepted: 10 November 2020; Published: 13 November 2020

Abstract: In an attempt to investigate the nature and origin of mantle heterogeneities beneath the South Mid-Atlantic Ridge (SMAR), we report new whole-rock Sr, Nd, Pb, and Hf isotopic data from eight basalt samples at four dredge stations along the SMAR between 18°S and 21°S. Sr, Nd, and Pb isotopic data from SMAR mid-ocean ridge basalts (MORBs) at 18–21°S published by other researchers were also utilized in this study. The SMAR MORBs at 18–21°S feature the following ratio ranges: $^{87}Sr/^{86}Sr$ = 0.70212 to 0.70410, $^{143}Nd/^{144}Nd$ = 0.512893 to 0.513177, $^{206}Pb/^{204}Pb$ = 18.05 to 19.50, $^{207}Pb/^{204}Pb$ = 15.47 to 15.71, $^{208}Pb/^{204}Pb$ = 37.87 to 38.64, and $^{176}Hf/^{177}Hf$ = 0.283001 to 0.283175. The $^{87}Sr/^{86}Sr$, $^{143}Nd/^{144}Nd$, $^{206}Pb/^{204}Pb$, and $^{176}Hf/^{177}Hf$ ratios of these MORBs varied considerably along the SMAR axis. The variable compositions of the Sr–Nd–Pb–Hf isotopes, combined with the corresponding whole-rock major and trace elemental abundances reported in previous studies, suggest that the SMAR MORBs at 18–21°S were probably derived from a heterogeneous mantle substrate related to a mixture of depleted mantle (DM) materials with a small amount (but variable input) of HIMU (high-μ, where μ = $^{238}U/^{204}Pb$)- and enriched (EMII)-type materials. The HIMU-type materials likely originated from the proximal St. Helena plume and may have been transported through "pipe-like inclined sublithospheric channels" into the SMAR axial zone. The EMII-type materials possibly originated from a recycled metasomatized oceanic crust that may have been derived from the early dispersion of other plume heads into the subcontinental asthenosphere prior to the opening of the South Atlantic Ocean. In addition, the contributions of subducted sediments, continental crust, and subcontinental lithospheric mantle components to the formation of the SMAR MORBs at 18–21°S may be nonexistent or negligible.

Keywords: Sr–Nd–Pb–Hf isotopes; mantle heterogeneities; plume–ridge interaction; St. Helena plume; South Mid-Atlantic Ridge

1. Introduction

Basaltic rocks that erupt along mid-ocean ridges (MORs) constitute the dominant volcanic rock type on the modern Earth (e.g., [1]). It is well established that mid-ocean ridge basalts (MORBs) originate from the partial melting of shallow-convecting asthenospheric mantle that is characterized by the significant depletion of incompatible trace elements (i.e., depleted upper mantle); these rocks are typically referred to as (normal) N-type mid-ocean ridge basalts (N-MORB) [2]. Variations in the chemical compositions of MORB suites have been interpreted to indicate complex mixing processes involving mantle heterogeneities that vary greatly in composition (e.g., [3–8], such as HIMU (high-μ, where $\mu = {}^{238}U/{}^{204}Pb$)-type components [9]), recycled mafic lithologies [10], and subcontinental lithospheric components (e.g., [2,11]). This mantle heterogeneity varies on different length scales ranging between ~1 and 1000 km [12–14].

Since the 1960s, mantle plume–ridge interactions have been a focal point in the field of geology because such interactions could play an important role in the formation of MORBs, whose compositions tend toward that of the proximal mantle plume (e.g., [6,15–19]). This process is one important reason why MORBs feature diverse mantle heterogeneities. Previous studies have demonstrated that basalts from the South Mid-Atlantic Ridge (SMAR; Figure 1a) are excellent examples for clarifying the isotopic variability of MORB mantle sources and mantle plume–ridge interactions, whose occurrences are well-documented in relation to the proximal Ascension, Circe, St. Helena, Tristan da Cunha, Gough, Discovery, and Shona plumes (e.g., [7,9–11,15,20–24]).

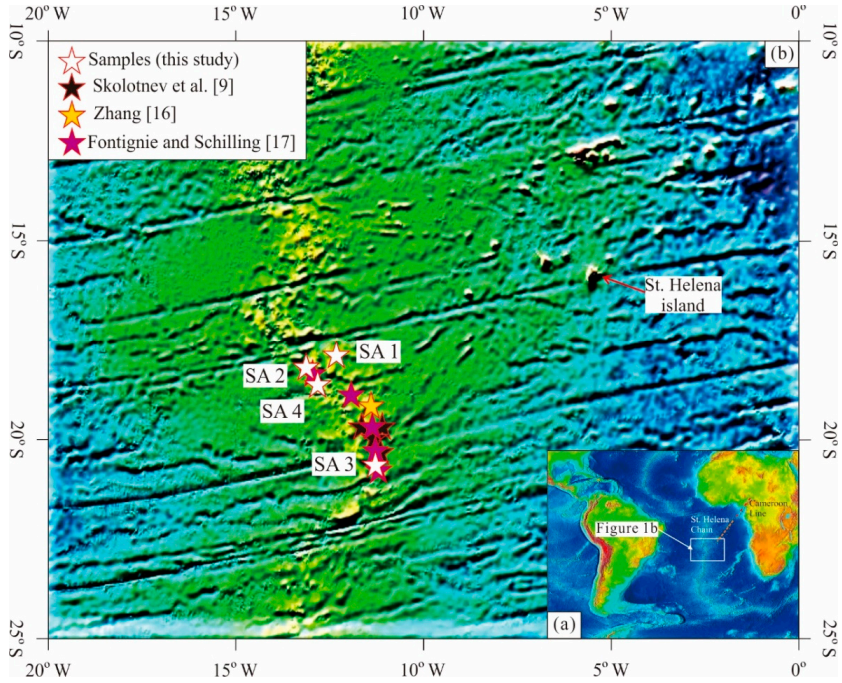

Figure 1. Map of the South Atlantic Mid-Ocean Ridge showing the dredged locations of the basalts analyzed in this study (map taken from [25]). (**a**) Map of the Atlantic Mid-Ocean Ridge showing the study area, (**b**) Sample location map.

The St. Helena (volcanic) island is located at a latitude of 16°S and a longitude of 5°43′W, nearly 800 km east of the SMAR (Figure 1b), and has an HIMU-type mantle plume origin (e.g., [26]). Basalts from the SMAR at 18–21°S are thus suitable for investigating the nature and extent of heterogeneities in the mantle beneath the SMAR and for constraining their mantle mixing process, such as the mantle plume–ridge interaction, due to their location adjacent to St. Helena island (Figure 1b). Based on the Sr–Nd–Pb isotopic analyses of basalts from the SMAR at 18–21°S, Fontignie and Schilling proposed that the production of these rocks may be related to a two-stage plume dispersion/melting

model that includes the earlier dispersion of the St. Helena plume head into the subcontinental asthenosphere and a later mantle plume–migrating ridge interaction [20]. This hypothesized mantle plume–ridge interaction beneath the SMAR between 18°S and 21°S is further supported by the fact that the SMAR MORBs at 19–20°S share some geochemical composition similarities (including Sr–Nd–Pb isotopes) with the proximal St. Helena plume [9,22]. The results of the seismic tomography support the existence of a flow channel connecting the SMAR with the St. Helena plume (e.g., [27]). This channel was previously proposed by [15,22] based on the geochemical component relationships between SMAR basalts and the St. Helena plume. However, according to the mineralogical, geochemical, and Sr–Nd isotopic signatures of basalts from the SMAR at 19°S, Zhang argued that these rocks were derived from a depleted mantle (DM) source with no mantle plume–ridge interaction [28]. Furthermore, Douglass et al. revealed the presence of so-called LOMU (low-μ) materials in the convecting mantle beneath the South Atlantic, according to the Sr, Nd, and Pb isotope variability along the SMAR at 40–55°S [16,29]. These components present a passive heterogeneity that represents a delaminated subcontinental lithospheric mantle that dispersed into the upper mantle that was related to the break-up of Gondwana and the subsequent opening of the South Atlantic Ocean [16]. In addition to the two-type components derived from the depleted asthenosphere and the St. Helena plume, our previous study based on whole-rock trace elements indicated that enriched materials derived from the subcontinental lithosphere mantle may also be involved in the genesis of the basalts from the SMAR at 18.0–20.6°S [30]. These conclusions indicate the possibility for Gondwana remnants in the upper mantle beneath the SMAR within the background section. In summary, (1) there is a plume–ridge interaction between the SMAR at 18–21°S and the St. Helena hotspot, that is, the St. Helena plume affects different segments of the SMAR at 18–21°S, and (2) the research on the kinds of enriched components involved in the formation of the SMAR MORBs at 18–21°S is still incomplete.

To describe the mantle heterogeneities in the study area, we analyzed Sr, Nd, Pb, and Hf isotopic data from eight dredged basalt samples (Figure 1b and Table 1). These samples had porphyritic textures and were previously analyzed for their mineralogy (olivine and plagioclase) and whole-rock major and trace elements [30], providing a petrological and geochemical framework with which we can discuss the Sr–Nd–Pb–Hf isotopic data. This study also included Sr, Nd, and Pb isotopic data from the SMAR MORBs at 18–21°S that were previously reported by [9,20,28] (Figure 1b and Table 1).

2. Geological Background

The Mid-Atlantic Ridge (MAR) is a submarine ridge composed of mountain chains lying along the north–south axis of the Atlantic Ocean. The MAR accounts for approximately 40% of the total global length of MORs and extends for ~16,000 km along a curvilinear path from the Arctic Ocean to near the southern tip of Africa (87°N to 54°S), and its width (1000–1500 km) accounts for one-third of the width of the Atlantic Ocean (e.g., [28,31,32]). It is considered a "slow-spreading" ridge due to its low average spreading rate of ~30 mm yr^{-1} (e.g., [31,33]). The MAR is divided into the North MOR and the SMAR and is separated by the near-equatorial Romanche Trench [31,34]. The SMAR is further divided into many relatively independent sections due to the influences of transform faults. Basalt constitutes the dominant volcanic rock type in the SMAR, together with local occurrences of peridotite, pyroxenite, and gabbro [31]. Mineralogical, whole-rock major and trace elemental and isotopic studies of SMAR basalts revealed that these rocks were generated with complex mixing processes and that their mantle compositions range widely from being geochemically depleted to apparently enriched (e.g., [2,9–11,16,20,35–37]).

Many off-ridge and ridge-centered hotspots, including the Ascension, Circe, St. Helena, Tristan da Cunha, Gough, Discovery, and Shona plumes, occur along the SMAR, and the components derived from these hotspots have likely played variable roles in the formation of SMAR basalts, such as plume–ridge interactions (e.g., [7,15,16,22]). St. Helena island (16°S) in the South Atlantic Ocean occurs adjacent to the study area (SMAR 18–21°S) (Figure 1b). This island is situated on a 39-Myr-old oceanic lithosphere [38] and reaches a height of 823 m above sea level, with a surface area of approximately

122 km^2 [39]. Bathymetric data indicate that St. Helena island, together with other adjacent seamounts, such as the Bonaparte seamount, constitute part of a scattered but nearly linear volcanic chain (the St. Helena Chain, Figure 1a) that results from the movement of the oceanic lithosphere above a mantle hotspot (e.g., [40,41]). Magma sources of volcanic rocks from St. Helena island yield low Rb/Sr, intermediate Sm/Nd, and high U/Pb parent/daughter ratios, and these rocks represent the HIMU-type endmember in the oceanic island basalt (OIB) compositional spectrum [42].

3. Analytical Methods

Samples were ground using an agate mortar and pestle to 200 mesh. Whole-rock Sr, Nd, Pb, and Hf isotopic analyses were performed at Nanjing FocuMS Technology Co., Ltd., China. The general analytical procedures are as follows:

(1) Rock powders were mixed with 0.5 mL of 60 wt.% HNO_3 + 1.0 mL of 40 wt.% HF in high-pressure PTFE (Poly tetra fluoroethylene) bombs. These bombs were steel-jacketed and subsequently placed in an oven at 195 °C for 3 days. Samples were placed on a hot plate until dry and were subsequently mixed with 1.5 mL of 0.2 N HBr + 0.5 N HNO_3 prior to ion exchange purification. (2) Pb was first collected using a Biorad AG1–X8 anion exchange column (Bio-Rad Laboratories, Hercules, CA, USA). Lithophile elements, including Sr, Hf, and rare earth elements (REEs), were initially washed from the column using a mixture of 0.2 N HBr + 0.5 N HNO_3 (collected), and Pb was then eluted with purified water. During this process, a second anion exchange column was needed to further purify/separate the Pb fraction because of the impurities within. (3) Sr, Hf, and REEs were separated using a Biorad AG50W–X8 cation exchange column (Bio-Rad Laboratories, Hercules, CA, USA). The lithophile elements collected in step (2) were dried and then redissolved in 1.5 N HCl through heating. High-field-strength elements (HFSEs, e.g., Ti, Zr, and Hf) were first washed out using 1.5 N HCl (collected); afterward, matrix elements (Na, Mg, K, and Ca) and Rb were separated using 2.0 N HCl (discarded). Sr fractions were collected using 2.5 N HCl before the REE fractions were finally retrieved using 6.0 N HCl (collected). (4) Hf was collected on a column using HDEHP(di(2-ethylhexyl)-coated Teflon powder. The HFSE Hf collected in step (3) was heated until dry and then redissolved in 3.0 N HCl. Ti was eluted using a mixture of 4.0 N HCl + 0.5 wt.% H_2O_2. Hf was finally extracted from the column using 2.0 N HF and collected in a 10 mL PFA (preconditioned perfluoroalkoxy) beaker. (5) The impure Sr fraction in step (3) was dried and subsequently redissolved in 2.5 N HNO_3 and then loaded into Sr-specific resin. Sr was finally extracted from the column with purified water. The Sr-specific resin was discarded after each chemical separation. (6) The REE fractions in step (3) were dried, redissolved in 0.12 N HCl, and loaded into another Ln-specific resin column. Light REEs (LREEs, e.g., La, Ce, and Pr) were first separated using 0.12 N HCl (discarded); afterward, Nd was collected using 0.18 N HCl, followed by Sm using 0.4 N HCl. (7) The Sr-, Nd-, Pb-, and Hf-bearing elutions were gently evaporated until dry and subsequently redissolved in 1.0 mL of 2 wt.% HNO_3. These diluted solutions were introduced into a Nu Plasma II MC–ICP–MS instrument (Wrexham, North Wales, UK) through an Aridus II desolvating nebulizer system (Teledyne Cetac Technologies, Omaha, NE, USA) to determine the whole-rock Sr–Nd–Pb–Hf isotopic compositions.

Raw data of isotopic ratios were internally corrected for mass fractionation by normalizing to $^{86}Sr/^{88}Sr = 0.1194$ for Sr, $^{146}Nd/^{144}Nd = 0.7219$ for Nd, $^{205}Tl/^{203}Tl = 2.3885$ for Pb, and $^{179}Hf/^{177}Hf = 0.7325$ for Hf using the exponential law. The following international isotopic standards were used for quality: NIST SRM 987 for Sr, JNdi-1 for Nd, NIST SRM 981 for Pb, and Alfa-Hf for Hf. The geochemical reference materials of USGS AGV-2 (andesite), BCR-2 (basalt), RGM-2 (rhyolite), and STM-2 (syenite) were used as quality controls for the Sr–Nd–Pb isotopes, along with those of USGS AGV-2 (andesite), BCR-2 (basalt), BHVO-2 (basalt), and STM-2 (syenite) for Hf isotopes. These isotopic results are consistent with previous publications and are within analytical uncertainty (Supplementary Table S1; [43,44]). The Sr, Nd, Pb, and Hf isotopic data of the SMAR basalt samples are listed in Table 1.

Table 1. Sr, Nd, Pb, and Hf isotope ratios in dredged basalts from the Southern Mid-Atlantic Ridge (18–21°S).

Sample	Latitude (°S)	Longitude (°W)	Depths (m)	$^{87}Sr/^{86}Sr$ ± 2 SE	$^{143}Nd/^{144}Nd$ ± 2 SE	$\varepsilon_{Nd}(t)$	$^{208}Pb/^{204}Pb$ ± 2 SE	$^{207}Pb/^{204}Pb$ ± 2 SE	$^{206}Pb/^{204}Pb$ ± 2 SE	$^{176}Hf/^{177}Hf$ ± 2 SE	$\varepsilon_{Hf}(t)$	ΔSr	Δ8/4Pb	Source
SA1A	18.04	12.85	3312	0.702516 ± 4	0.513139 ± 2	9.8	38.4175 ± 13	15.6137 ± 5	18.7678 ± 5	0.2831397 ± 2	13.0	25.16	10.03	This paper
SA1B	18.04	12.85	3312	0.702491 ± 3	0.513147 ± 2	9.9	38.3223 ± 13	15.5984 ± 5	18.5982 ± 6	0.2830365 ± 2	9.4	24.91	21.01	
SA2A	18.02	12.92	3386	0.702567 ± 3	0.513123 ± 3	9.5	38.5225 ± 12	15.7089 ± 4	19.5033 ± 4	0.2831724 ± 2	14.2	25.67	−68.40	
SA2B	18.02	12.92	3386	0.702517 ± 4	0.513148 ± 2	9.9	38.3612 ± 11	15.6453 ± 4	18.8627 ± 3	0.2831754 ± 2	14.3	25.17	−7.08	
SA3A	20.57	11.65	3302	0.702553 ± 4	0.513113 ± 2	9.3	38.4306 ± 12	15.6487 ± 4	18.6470 ± 4	0.2831554 ± 1	13.6	25.53	25.93	
SA3B	20.57	11.65	3302	0.702689 ± 5	0.513096 ± 2	8.9	38.4903 ± 13	15.6450 ± 4	18.8954 ± 5	0.2831281 ± 1	12.6	26.89	1.87	
SA4A	18.71	12.67	2386	0.703213 ± 5	0.513064 ± 2	8.3	38.6411 ± 16	15.6517 ± 5	18.8388 ± 5	0.2830007 ± 2	8.1	32.13	23.80	
SA4B	18.71	12.67	2386	0.702898 ± 4	0.513046 ± 2	8.0	38.6338 ± 12	15.6442 ± 4	18.8872 ± 4	0.2831143 ± 2	12.1	28.98	17.22	
S029-TVG23	19.50	11.99	2700	0.70299	0.513116	9.3						29.90		Zhang [28]
S032-TVG26	19.42	12.00	2407	0.70286	0.513127	9.5						28.60		
S033-TVG27	19.40	11.97	2475	0.70291	0.513125	9.5						29.10		
S035-TVG28	19.41	11.93	2590	0.70291	0.513098	9.0						29.10		
S039-TVG31	19.50	11.98	2652	0.70312	0.513117	9.3						31.20		
S028-TVG22	19.57	11.98	2699	0.7034	0.513019	7.4						34.00		
S031-TVG25	19.46	11.96	2530	0.70301	0.513017	7.4						30.10		
S030-TVG24	19.53	11.94	2825	0.70301	0.513108	9.2						30.10		
S036-TVG29	19.38	11.94	2796	0.7028	0.513144	9.9						28.00		
S037-TVG30	19.34	11.93	2546	0.703	0.513071	8.4						30.00		
S042-TVG33	19.34	11.93	2638	0.70288	0.513177	10.5						28.80		
S043-TVG34	19.34	11.93	2477	0.7029	0.513153	10.0						29.00		
S044-TVG35	19.34	11.93	2486	0.70282	0.513148	9.9						28.20		
I1050/8	20.00	12.07	2400–2100	0.702967	0.513097	9.0	38.395	15.534	19.022			24.11	−22.96	Skolotnev et al. [9]
I1050/10	20.00	12.07	2400–2100	0.702604	0.512971	6.5	38.075	15.579	18.155			24.53	49.86	
I1049/21	20.00	11.78	2800-2200	0.703027	0.512893	5.0	37.903	15.483	18.384			23.97	4.97	
I1051/3	20.20	11.84	3500–3200	0.702502	0.513016	7.4	37.874	15.548	18.046			22.14	42.94	
I1052/6	20.40	11.70	3200–3100	0.702912	0.512939	5.9	38.149	15.467	18.412			24.13	26.19	
EN061 22D-1G	18.38	12.84	3675	0.702411 ± 26	0.513154 ± 3		38.091 ± 15	15.546 ± 6	18.727 ± 7			29.67	−17.69	Fontignie and Schilling [20] and Hanan et al. [22]
EN061 23D-1G	18.98	12.30	3537	0.702453 ± 36	0.513075 ± 2		38.291 ± 58	15.563 ± 24	18.786 ± 28			26.04	−4.83	
EN063 1D-6G	20.79	11.60	3460	0.702397 ± 9	0.513073 ± 8		37.969 ± 70	15.511 ± 24	18.533 ± 23			30.27	−6.44	
2IID 26D-2G	19.99	11.88	3560	0.702214 ± 6	0.513118 ± 3		37.937 ± 17	15.505 ± 8	18.542 ± 8			25.02	−10.73	
EN061 25D-1G	20.32	11.71	3270	0.702413 ± 7	0.513089 ± 3		37.960 ± 38	15.523 ± 13	18.523 ± 13			29.12	−6.13	

Note: $\Delta Sr = [(^{87}Sr/^{86}Sr)_{DS} - 0.7] \times 10^4$; $\Delta 8/4Pb = [(^{208}Pb/^{204}Pb)_{DS} - (^{208}Pb/^{204}Pb)_{NHRL}] \times 10^2$; NHRL—Northern Hemisphere Reference Line; DS—the magnitude of the isotopic anomaly of any given data set [45].

4. Results

The MORBs from the SMAR between 18–21°S exhibited a relatively wide range of whole-rock Sr, Nd, Pb, and Hf isotopic compositions (Table 1). These rocks yielded $^{206}Pb/^{204}Pb$ = 18.05–19.50, $^{207}Pb/^{204}Pb$ = 15.47–15.71, and $^{208}Pb/^{204}Pb$ = 37.87–38.64, along with $^{87}Sr/^{86}Sr$ = 0.702214–0.703400, $^{143}Nd/^{144}Nd$ = 0.512893–0.513177, and $^{176}Hf/^{177}Hf$ = 0.283001–0.283175. The corresponding $\varepsilon_{Nd}(t)$ and $\varepsilon_{Hf}(t)$ values were +5.0 to +10.5 and +8.1 to +14.1, respectively. The Sr, Nd, Pb, and Hf isotopic data of these MORBs fell into the range of Atlantic MORB on a variety of correlation diagrams: $^{87}Sr/^{86}Sr$ versus $^{143}Nd/^{144}Nd$ (Figure 2a), $^{206}Pb/^{204}Pb$ versus $^{208}Pb/^{204}Pb$ (Figure 2b), $^{206}Pb/^{204}Pb$ versus $^{207}Pb/^{204}Pb$ (Figure 2c), $^{206}Pb/^{204}Pb$ versus $^{87}Sr/^{86}Sr$ (Figure 3a), $^{206}Pb/^{204}Pb$ versus $^{143}Nd/^{144}Nd$ (Figure 3b), $^{143}Nd/^{144}Nd$ versus $^{176}Hf/^{177}Hf$ (Figure 4a), and $^{206}Pb/^{204}Pb$ versus $^{176}Hf/^{177}Hf$ (Figure 4b). Furthermore, as shown in Figure 2b,c, the basalts formed a roughly parallel trend to the Northern Hemisphere Reference Line (NHRL [45]) but roughly plot above this line with relatively high $^{208}Pb/^{204}Pb$ and $^{207}Pb/^{204}Pb$ ratios at a moderate $^{206}Pb/^{204}Pb$ ratio. In addition, these rocks yielded $^{87}Sr/^{86}Sr$ = 0.702214–0.703400 (<0.7050), ΔSr = 22.14–34.00 (<50), and Δ8/4Pb = –68.40 to 49.86 (<60) (the equations of ΔSr and Δ8/4Pb are presented in Table 1 [45]), which are different from the typical Dupal anomaly in the Southern Hemisphere [45,46]. This feature was further supported by the fact that these MORBs plotted far from the field of Dupal OIBs on the $^{206}Pb/^{204}Pb$ versus $^{208}Pb/^{204}Pb$ diagram (Figure 2b).

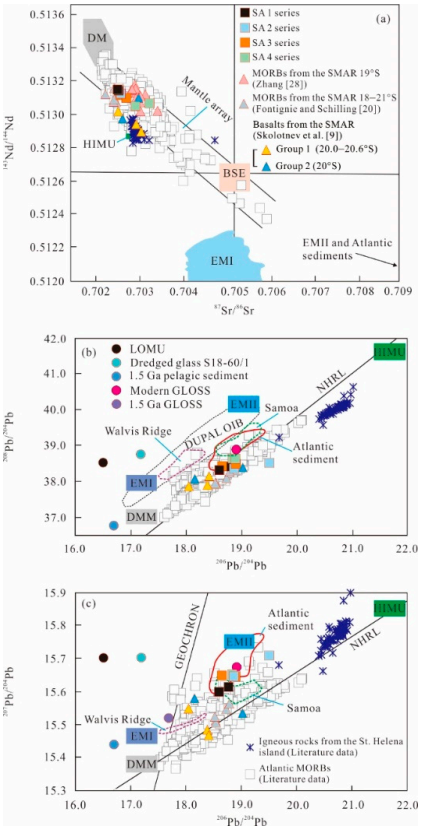

Figure 2. $^{87}Sr/^{86}Sr$ versus $^{143}Nd/^{144}Nd$ (**a**), $^{206}Pb/^{204}Pb$ versus $^{208}Pb/^{204}Pb$ (**b**), and $^{206}Pb/^{204}Pb$ versus $^{207}Pb/^{204}Pb$ diagrams (**c**) (after [42,47] and references therein) of the basalts from the South Mid-Atlantic Ridge (SMAR) at 18–21°S. The Atlantic mid-ocean ridge basalt (MORB) and the St. Helena magmatic rock values are from http://georoc.mpch-mainz.gwdg.de/georoc/Entry.html. The Atlantic sediment values are from [48–50]. The LOMU (low-μ) endmember values are from [11]. The 1.5 Ga pelagic sediment values are from [51]. The modern and 1.5 Ga global subduction sediment (GLOSS) values are from [52]. The dredged glass S18-60/1 from the SMAR at ~54.5°S is from [11]. DMM—depleted MORB mantle, EM—enriched mantle, HIMU—high μ, OIB—oceanic island basalt.

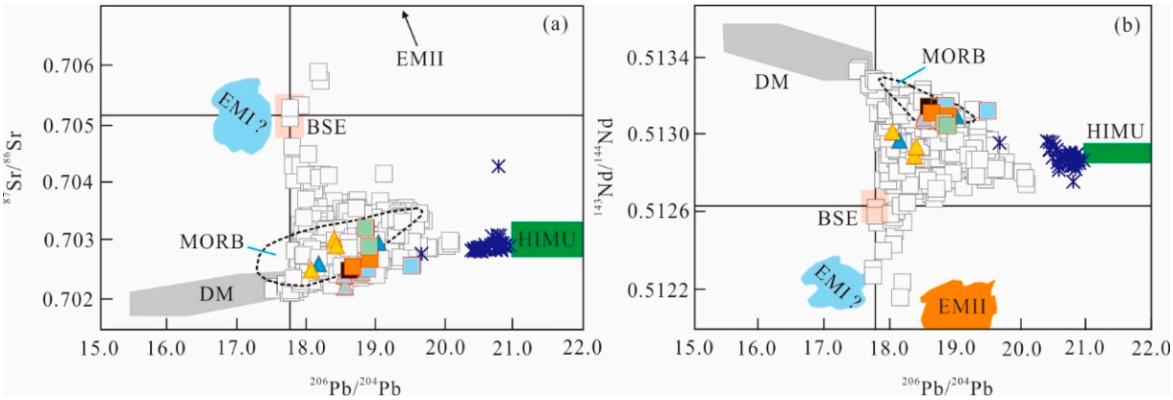

Figure 3. $^{206}Pb/^{204}Pb$ versus $^{87}Sr/^{86}Sr$ (**a**) and $^{206}Pb/^{204}Pb$ versus $^{143}Nd/^{144}Nd$ (**b**) diagrams (after [53]) of the basalts from the SMAR at 18–21°S. The Atlantic MORB and the St. Helena igneous rock values are from http://georoc.mpch-mainz.gwdg.de/georoc/Entry.html. Symbols are the same as in Figure 2.

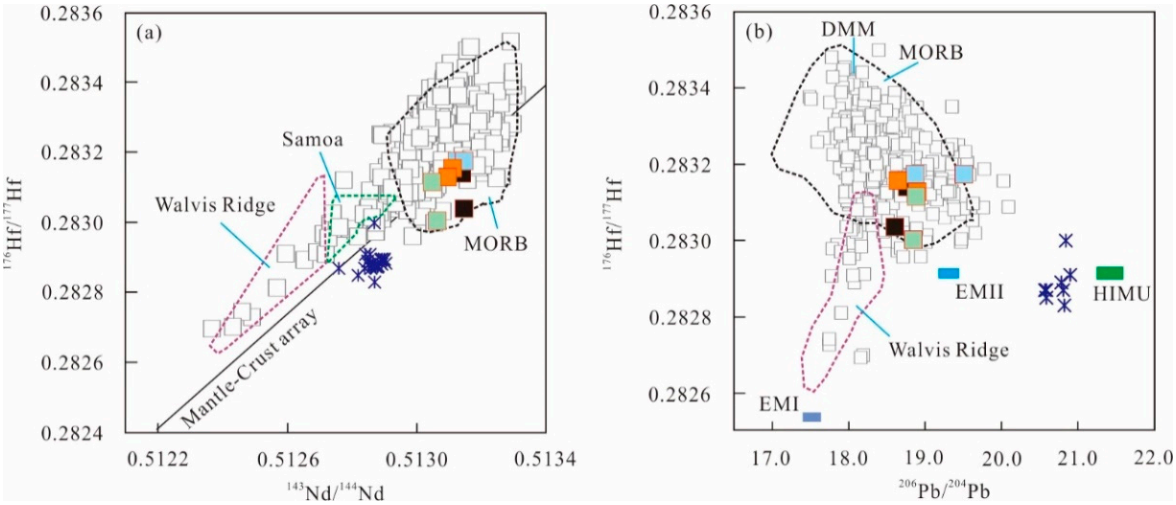

Figure 4. $^{143}Nd/^{144}Nd$ versus $^{176}Hf/^{177}Hf$ (**a**) and $^{206}Pb/^{204}Pb$ versus $^{176}Hf/^{177}Hf$ (**b**) diagrams (after [42,47,54] and references therein) of the basalts from the SMAR at 18–21°S. The Atlantic MORB and the St. Helena igneous rock values are from http://georoc.mpch-mainz.gwdg.de/georoc/Entry.html. Symbols are the same as in Figure 2.

The latitudinal variations in the Sr–Nd–Pb–Hf isotope ratios are displayed in Figure 5, showing that the $^{87}Sr/^{86}Sr$, $^{143}Nd/^{144}Nd$, $^{206}Pb/^{204}Pb$, and $^{176}Hf/^{177}Hf$ ratios of the MORBs from the SMAR at 18–21°S varied considerably along the SMAR axis. It is clear that these ratios were different from those of the depleted MORB mantle (DMM; $^{87}Sr/^{86}Sr$ = 0.7020–0.7024, $^{143}Nd/^{144}Nd$ = 0.5131–0.5133, $^{206}Pb/^{204}Pb$ = 15.5–17.8, and $^{176}Hf/^{177}Hf$ = 0.2831–0.2835 [42]) and the average MORB ($^{87}Sr/^{86}Sr$ = 0.702819, $^{143}Nd/^{144}Nd$ = 0.513074, $^{206}Pb/^{204}Pb$ = 18.412, and $^{176}Hf/^{177}Hf$ = 0.283 [55]) (Figure 5). These characteristics, combined with those of the SMAR MORBs at 18–21°S, plotted far from the DM/DMM endmember in Figures 2 and 3, suggesting that these rocks were not simply derived from a DM source.

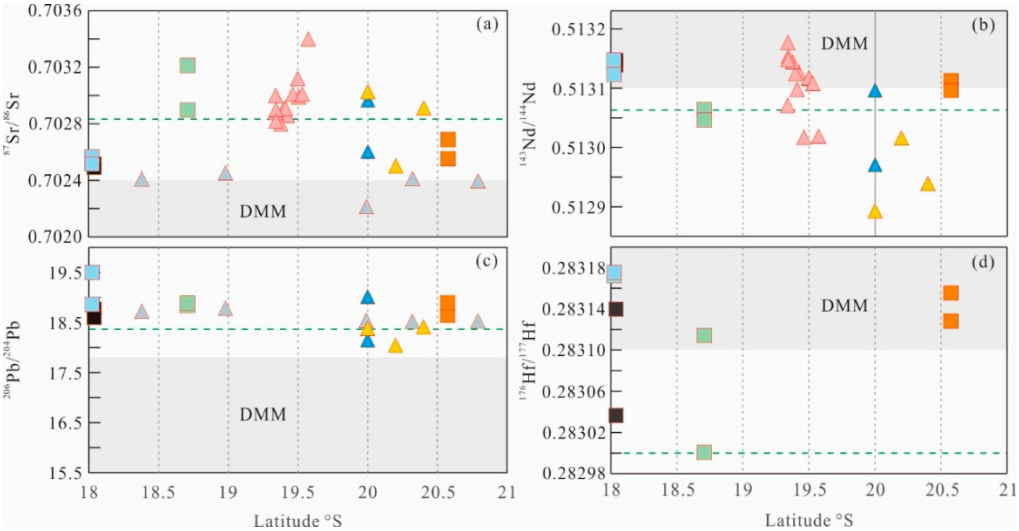

Figure 5. Comparison of the latitudinal variations in $^{87}Sr/^{86}Sr$, $^{143}Nd/^{144}Nd$, $^{206}Pb/^{204}Pb$, and $^{176}Hf/^{177}Hf$ in the basalts from the SMAR at 18–21°S. The DMM values are from [42]. The green dotted line represents the average MORB isotopic composition from [55], with $^{87}Sr/^{86}Sr$ = 0.702819 (n = 272), $^{143}Nd/^{144}Nd$ = 0.513074 (n = 272), $^{206}Pb/^{204}Pb$ = 18.412 (n = 245), and $^{176}Hf/^{177}Hf$ = 0.283 (n = 138). Symbols are the same as in Figure 2. In Figure 5, the basalts from the SMAR at 18–21°S have broad ranges of $^{87}Sr/^{86}Sr$ (**a**), $^{143}Nd/^{144}Nd$ (**b**), and $^{176}Hf/^{177}Hf$ (**d**) ratios relative to those of the DMM and the average MORB and yield $^{206}Pb/^{204}Pb$ ratios mostly higher than those of the DMM and the average MORB (**c**).

5. Discussion

5.1. MORBs from the SMAR at 18–21°S Originated from a Heterogeneous Mantle Source

MORBs are derived from decompression melting of the upper mantle, but this melting process can be complex and generates diverse geochemical characteristics [56]. Incompatible trace elements and Sr–Nd–Pb–Hf isotopes are powerful tools for determining the mantle sources involved in the genesis of MORBs. Previous studies indicated that the SMAR MORBs at 18–21°S show N-MORB- and enriched-type mid-ocean ridge basalt (E-MORB)-like geochemical compositions that suggest a complex magma source in this area [9,28,30]. The diverse radiogenic isotopic compositions observed in MORBs are usually ascribed to chemical heterogeneity in the mantle [56]. The MORBs from the SMAR at 18–21°S originated from the mixing of depleted and enriched source components, which are shown on the $^{87}Sr/^{86}Sr$ versus $^{143}Nd/^{144}Nd$ diagram (Figure 2a). In agreement with the Nd–Sr isotope correlation, the covariations of $^{206}Pb/^{204}Pb$ versus $^{208}Pb/^{204}Pb$, $^{206}Pb/^{204}Pb$ versus $^{207}Pb/^{204}Pb$, $^{206}Pb/^{204}Pb$ versus $^{87}Sr/^{86}Sr$, and $^{206}Pb/^{204}Pb$ versus $^{143}Nd/^{144}Nd$ (Figure 2b,c and Figure 3) confirmed the mixing of depleted and enriched materials. These signatures revealed that the SMAR MORBs at 18–21°S did not originate from a DM source but from a heterogeneous mantle source. Although these basalts extended from depleted to enriched endmembers in these plots, most of the basalts feature N-MORB-like geochemical characteristics (Figure 6) [9,28,30], meaning they were mainly derived from a DM source with some contributions of enriched components.

5.2. Mixing Components in the MORBs from the SMAR at 18–21°S

The chemical heterogeneity within the derived MORBs is assumed to be a result of plume–ridge interactions [2,15,22]. The South Atlantic upper mantle appears to contain an ambient large ion lithophile element (LILE)-depleted upper mantle. This geochemical profile (including radioisotopes) may have been triggered by broad contamination of the depleted upper mantle (e.g., [7,16]). Several mechanisms for this are proposed: (1) dispersion of solid residue from prior partial melting of a mantle plume

head, where this could relate to melting before the break-up of Gondwana and consist of recycled metasomatized oceanic crust, pelagic sediments, and harzburgite matrix; (2) dispersion of delaminated continental materials (sub-Gondwanan lithosphere or lower crustal blocks) during the break-up of Gondwana and opening of the Atlantic; (3) dispersion of supra-subduction mantle wedge components that were previously altered by subduction zone-related fluids or melts over an ancient subduction zone; (4) a transition zone from the normal North Atlantic/Pacific-type MORB source to the Dupal-type upper mantle source (e.g., [7,11,16,20,36,37,45,57]).

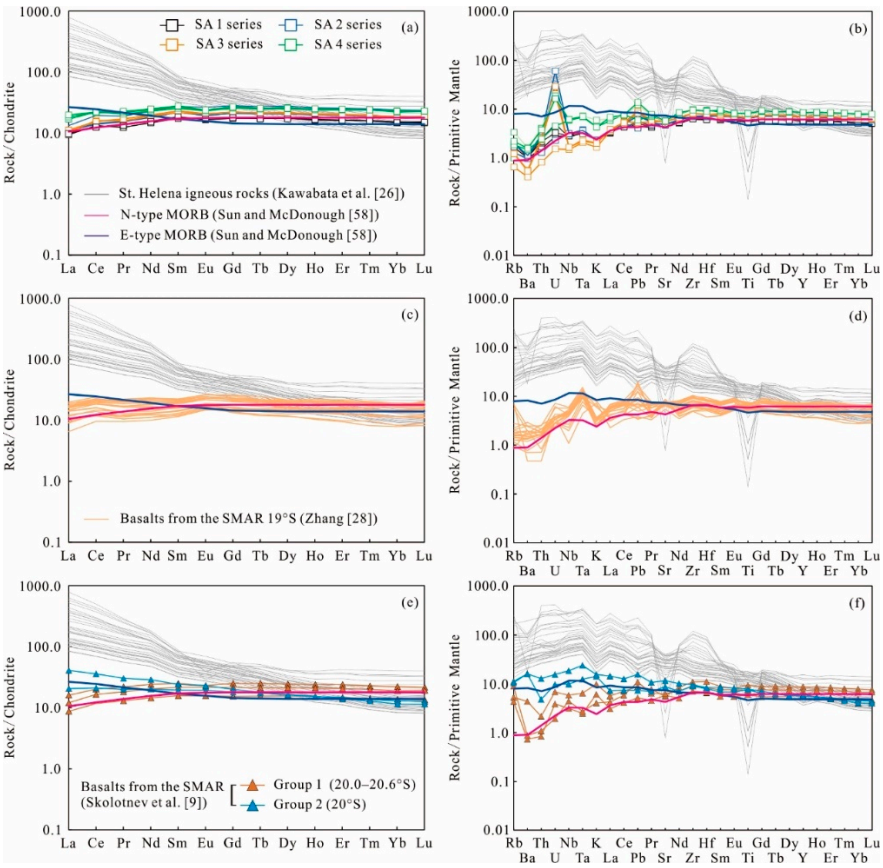

Figure 6. Chondrite-normalized REE (**a**–**e**) and primitive mantle-normalized multielement (**b**–**f**) diagrams of the basalts from the SMAR at 18–21°S. The chondrite and primitive mantle normalization data are from [58]. (**e**,**f**) according to Skolotnev et al. [9], the formation of the group 1 basalts resembles that of the depleted OIB associated with the melting of a mantle substrate dominated by DMM-type components and the group 2 basalts were derived from a heterogeneous mantle substrate that was linked to the mixing of DM components with HIMU-type components, which are possibly related to the spreading of mantle material of the St. Helena plume.

On the $^{87}Sr/^{86}Sr$ versus $^{143}Nd/^{144}Nd$ diagram (Figure 2a), the MORBs from the SMAR at 18–21°S had a relatively large variation in these isotopic ratios, which possibly required some form of mixing of three isotopically distinct mantle endmembers that included DM, HIMU, and enriched mantle (EM) reservoirs. In particular, some samples were plotted into and around the HIMU field in this diagram. Plots involving Pb isotopes are quite accurate in determining the roles played by EM and HIMU reservoirs because the rocks derived from these sources yield very different isotopic features from N-MORB. On the $^{206}Pb/^{204}Pb$ versus $^{208}Pb/^{204}Pb$ diagram (Figure 2b), an apparent mixing array can be identified that starts from the DMM endmember and points in the direction of an HIMU-type source. On the $^{206}Pb/^{204}Pb$ versus $^{207}Pb/^{204}Pb$ diagram (Figure 2c), the MORB data trend does not pass through the HIMU field but confirmed the mixing of the three isotopically distinct mantle reservoirs of DMM, HIMU, and EM. In addition, the $^{206}Pb/^{204}Pb$ versus $^{87}Sr/^{86}Sr$ and $^{206}Pb/^{204}Pb$ versus $^{143}Nd/^{144}Nd$

diagrams (Figure 3) further indicated the mixing of the components of depleted and enriched (HIMU + EM) endmembers. Thus, the Sr–Nd–Pb–Hf isotopes strongly supported a three-component (DM + HIMU + EM) mantle-mixing model for the genesis of the MORBs from the SMAR at 18–21°S. This inference is consistent with our previous conclusion that the SMAR MORBs at 18.0–20.6°S were likely derived from a DM source with the contribution of enriched materials based on analyses of the corresponding whole-rock major and trace element compositions [30].

5.2.1. EM-Type Components

In Figures 2, 3 and 4b, the Sr–Nd–Pb–Hf isotopes indicate that EMII-type (with few or no EMI-type) components were possibly involved in the origin of the MORBs from the SMAR at 18–21°S. These features indicate that enriched materials, such as subducted (pelagic or terrigenous) sediments, metasomatized oceanic crust, continental crust, or metasomatized mantle, may have been involved in the genesis of these rocks (e.g., [42,53,59–63]).

Pb isotopic systematics can be used to test the model of marine sediment addition. In Figure 2b,c, some samples of the SA 1–4 series in this study fell into the field of Atlantic sediments that were close to or near the modern global subduction sediment (GLOSS) field due to their relatively high $^{208}Pb/^{204}Pb$ and $^{207}Pb/^{204}Pb$ ratios for a given $^{206}Pb/^{204}Pb$ value. These signatures suggest that marine sediments influenced the geochemical profile of these rocks. Several lines of evidence demonstrate that only minor amounts of oceanic sediment could have contributed to the generation of SMAR MORBs at 18–21°S: (1) The MORBs plot far from the 1.5 Ga pelagic sediment and GLOSS fields in Figure 2b,c. (2) Their low $^{87}Sr/^{86}Sr$ ratios (0.702214–0.703400) but high $^{143}Nd/^{144}Nd$ ratios (0.512893–0.513177), $^{176}Hf/^{177}Hf$ ratios (0.283001–0.283175), and $\varepsilon_{Nd}(t)$ (5.0–10.5) and $\varepsilon_{Hf}(t)$ (8.1–14.3) values (Table 1) were different from those of the 1.5 Ga, modern GLOSS and 1.5 Ga pelagic sediments (Table 2). (3) These MORBs yielded much lower $(Th/Nb)_{PM}$ (the subscript "PM" indicates normalization to the primitive mantle value) ratios (0.33–1.58) [28,30]) than the average GLOSS value (6.5) [52]. (4) The majority of these MORBs were extremely depleted in Ba, as shown in Figure 6. Coincidentally, in addition to the two SA 3 series samples (with weak negative Nb–Ta anomalies; Figure 6), which plotted slightly above the mantle array due to their relatively high Th/Yb ratios for a given Nb/Yb, the other SMAR MORBs at 18–21°S plotted within the MORB array field on the Nb/Yb versus Th/Yb diagram (not shown) [30], confirming the negligible role of subduction components (e.g., sediments) in the genesis of these MORBs.

Table 2. Sr, Nd, Pb, and Hf isotopes of three endmember components.

Sample	Modern GLOSS	1.5 Ga Pelagic Sediments	1.5 Ga GLOSS
$^{87}Sr/^{86}Sr$	0.71730	0.7203	0.713587
$^{143}Nd/^{144}Nd$	0.51218	0.5117	0.511977
$\varepsilon_{Nd}(t)$	−8.9		
$^{206}Pb/^{204}Pb$	18.913	16.7	17.69
$^{207}Pb/^{204}Pb$	15.673	15.44	15.52
$^{208}Pb/^{204}Pb$	38.899	36.8	
$^{176}Hf/^{177}Hf$	0.282829	0.2826	0.282228
$\varepsilon_{Hf}(t)$	+2 (±3)		

Note: The modern GLOSS values are from [52,64]. The 1.5 Ga pelagic sediment values are from [51]. The 1.5 Ga GLOSS values are from [7,52].

According to previous studies, some MORB samples from the SMAR at 18–21°S (e.g., SA 3 series) displayed a depletion of Nb and/or Ta compared to neighboring elements on the chondrite-normalized REE and primitive mantle-normalized multielement diagrams (Figure 6). These features may suggest contamination by a continental crust or a subcontinental lithospheric mantle [65–68]. Crustal components are characterized by the enrichment of LILEs and LREEs and the depletion of Nb, Ta, and Ti [69]. Minor crustal involvement in magmas can result in Nb–Ta depletions and

Zr–Hf enrichments compared to neighboring elements [70]. As shown in Figure 6, there were no obviously positive Zr–Hf or negative Ti anomalies. These characteristics, combined with the fact that most MORB samples were marked by LREE-depleted patterns, the apparent depletion of Ba and the lack of negative Nb–Ta compared to neighboring elements (Figure 6) supported negligible crustal involvement. Furthermore, the continental crust is enriched in Th with high Th/La ratios of ~0.30 [71] and Th/Ce ratios of ~0.15 [72], in contrast to mantle-derived magmas, which record values of ~0.12 and 0.02–0.05, respectively [58]. The MORBs from the SMAR at 18–21°S showed weak to apparent negative Th anomalies (Figure 6) and yielded significantly lower Th/La (0.03–0.11) and Th/Ce (0.01–0.05) ratios, resembling mantle-derived melts, further revealing the negligible or nonexistent occurrence of continental crustal addition.

Previous studies proposed the existence of a LOMU component dispersed in the South Atlantic convecting asthenospheric mantle, where this component in MORBs is possibly a feature of the South Atlantic [16,29]. The LOMU component is marked by low $^{206}Pb/^{204}Pb$, $^{208}Pb/^{204}Pb$, and $^{143}Nd/^{144}Nd$ ratios, high $^{87}Sr/^{86}Sr$ ratios, and variable $^{207}Pb/^{204}Pb$ ratios, and represents a delaminated subcontinental lithospheric mantle due to the impact of a mantle plume during the break-up of Gondwana [16,73]. Douglass and Schilling reported the Sr–Nd–Pb isotopes of the LOMU material with $^{87}Sr/^{86}Sr$ = 0.71000, $^{143}Nd/^{144}Nd$ = 0.51125, $^{206}Pb/^{204}Pb$ = 16.50, $^{207}Pb/^{204}Pb$ = 15.70, and $^{208}Pb/^{204}Pb$ = 38.50 [11]. The MORBs from the SMAR at 18–21°S displayed low $^{87}Sr/^{86}Sr$ ratios (0.702214–0.703400) but high $^{143}Nd/^{144}Nd$ (0.512893–0.513177) ratios (Table 1), which were different from the LOMU component. Again, these rocks yielded $^{206}Pb/^{204}Pb$ = 18.05–19.50, $^{207}Pb/^{204}Pb$ = 15.47–15.71, and $^{208}Pb/^{204}Pb$ = 37.87–38.64 (Table 1), which plotted far from the LOMU field on the $^{206}Pb/^{204}Pb$ versus $^{208}Pb/^{204}Pb$ (Figure 2b) and $^{206}Pb/^{204}Pb$ versus $^{207}Pb/^{204}Pb$ (Figure 2c) diagrams. In addition, Kamenetsky et al. [37] proposed that the Sr–Nd–Pb isotopic ratios of dredged glass S18-60/1 from the SMAR near the Bouvet Triple Junction at ~54.5°S closely resemble those of the LOMU component with $^{87}Sr/^{86}Sr$ = 0.712090, $^{143}Nd/^{144}Nd$ = 0.511663, $^{206}Pb/^{204}Pb$ = 17.188, $^{207}Pb/^{204}Pb$ = 15.701, and $^{208}Pb/^{204}Pb$ = 38.766 [11]. This glass was possibly derived from lower crustal fragments stranded in the upper mantle during the break-up of Gondwana and the opening of the Atlantic [37]. The SMAR MORBs at 18–21°S had $^{87}Sr/^{86}Sr$ ratios of 0.702214–0.703400 and $^{143}Nd/^{144}Nd$ ratios of 0.512893–0.513177 (Table 1), which were different from those of glass S18-60/1 and also plotted far from the glass S18-60/1 field in Figure 2b,c due to their relatively low $^{207}Pb/^{204}Pb$ (15.47–15.71) and $^{208}Pb/^{204}Pb$ (37.87–38.64) ratios for given $^{06}Pb/^{204}Pb$ ratios (18.05–19.50) (Table 1). From these results, we concluded that no or only negligible amounts of LOMU-type materials (sub-Gondwanan lithosphere or lower crustal blocks) were involved in the genesis of the MORBs from the SMAR at 18–21°S.

According to previous studies, we note that some MORB samples from the SMAR at 18–21°S have the following features [9,28,30]: (1) selectively depleted in trace (e.g., Ba, Th, Nb, and Ta) and heavy REE (HREE, e.g., Yb and Lu) elements compared to N-MORBs on chondrite-normalized REE and primitive mantle-normalized multielement diagrams (Figure 6), and (2) apparent depletion of Rb, Ba, and Th compared to U, along with the remarkable depletion of K (Figure 6). Together with the MORBs from the SMAR at 18–21°S yielding low $^{87}Sr/^{86}Sr$ ratios (0.702491–0.703400) and positive $\varepsilon_{Nd}(t)$ (+5.0 to +10.5) and $\varepsilon_{Hf}(t)$ (+8.1 to +14.1) values (Table 1) and the discussion for EM-type components above, these signatures revealed that the small amounts of EMII-type materials contributed to the genesis of MORBs from the SMAR at 18–21°S and may be derived from a recycled metasomatized oceanic crust. This inference may be supported by the fact that recycled mafic lithologies were involved in the production of MORBs at 5–11°S along the SMAR based on U–Th–Ra disequilibria data [10].

5.2.2. HIMU-Type Components

As shown in Figure 6, some MORB samples (e.g., SA 4 series samples and group 2 samples from the SMAR at 20°S reported by Skolotnev et al. [9]) from the SMAR at 18–21°S featured positive Nb–Ta anomalies compared to N-MORBs. These signatures, together with the group 2 MORBs from the SMAR at 20°S, exhibited E-MORB-like geochemical compositions (Figure 6) [9], and some MORB

samples plotted into and around the Iceland array zone in Figure 7 [74], indicating the possible role of a mantle plume in the genesis of these rocks.

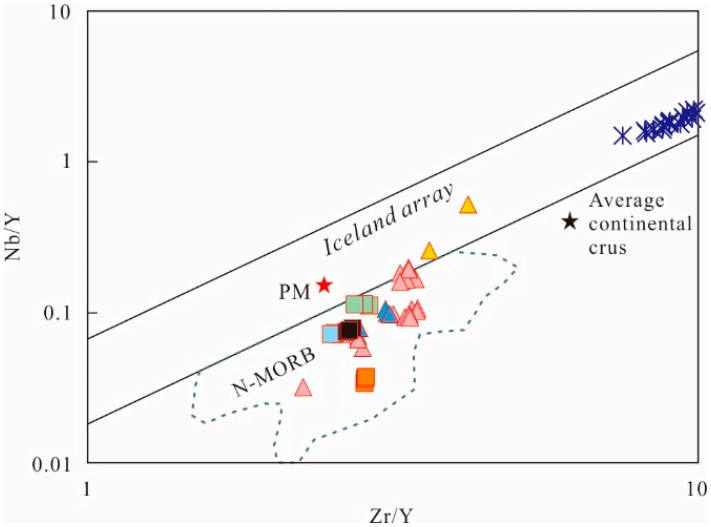

Figure 7. Nb/Y versus Zr/Y diagram (after [74] and references therein) of the basalts from the SMAR at 18–21°S. The data are from [9,28,30]. The parallel lines indicate the lower and upper limits of the Iceland data array. The lower line with ΔNb = 0 (ΔNb = 1.74 + log(Nb/Y) –1.92 log(Zr/Y), representing the deficiency or excess in Nb relative to the lower line) separates the parallel Icelandic (ΔNb > 0) and N-type mid-ocean ridge basalts (N-MORB; ΔNb < 0). Symbols are the same as in Figure 2.

St. Helena island, which is adjacent to the SMAR at 18–21°S, is a HIMU-type hotspot oceanic island in the South Atlantic Ocean [75]. Previous studies proposed that components derived from the St. Helena hotspot played an important role in the production of South Atlantic MORBs based on the Sr–Nd–Pb–He isotopes (e.g., [6,9,20,22]). Figures 2–4 depict the isotopic compositional fields of magmatic rocks from St. Helena island. Although the MORBs from the SMAR at 18–21°S differed in the Sr–Nd–Pb–Hf isotopes from the St. Helena magmatic rocks, these rocks showed a clear isotopic trend toward the St. Helena igneous rocks on the $^{87}Sr/^{86}Sr$ versus $^{143}Nd/^{144}Nd$, $^{206}Pb/^{204}Pb$ versus $^{208}Pb/^{204}Pb$, $^{206}Pb/^{204}Pb$ versus $^{207}Pb/^{204}Pb$, $^{206}Pb/^{204}Pb$ versus $^{87}Sr/^{86}Sr$, $^{206}Pb/^{204}Pb$ versus $^{143}Nd/^{144}Nd$, $^{143}Nd/^{144}Nd$ versus $^{176}Hf/^{177}Hf$, and $^{206}Pb/^{204}Pb$ versus $^{176}Hf/^{177}Hf$ diagrams (Figures 2–4). These features are consistent with the SMAR MORBs at 18–21°S, which show a similar trend toward St. Helena igneous rocks on the Nb/Yb versus Th/Yb and La/Sm versus Sm/Yb diagrams (not shown) [30]. Therefore, the Sr–Nd–Pb–Hf isotopic compositions of the MORBs from the SMAR at 18–21°S confirmed the probable influence of components derived from the St. Helena plume in their diagenetic processes but with small and varying degrees of contributions for rocks at different locations.

On the basis of the geochemical compositions discussed above, we concluded that three types of sources were possibly involved in the genesis of the SMAR MORBs at 18–21°S: (1) depleted mantle, (2) EMII-type materials derived from recycled metasomatized oceanic crust, and (3) HIMU-type components derived from the St. Helena hotspot. To further estimate the involved endmembers and their relative proportions, several quantitative trace element and isotope mixing models were used in this study (Figure 8). Quantitative modeling indicates that the compositions of the SMAR MORBs at 18–21°S can be produced mainly by the melting of a mantle source consisting of >80% depleted mantle materials combined with small quantities of St. Helena hotspot components (Figure 8). The contribution of EMII-type components could be minor with no input of LOMU-type materials (Figure 8).

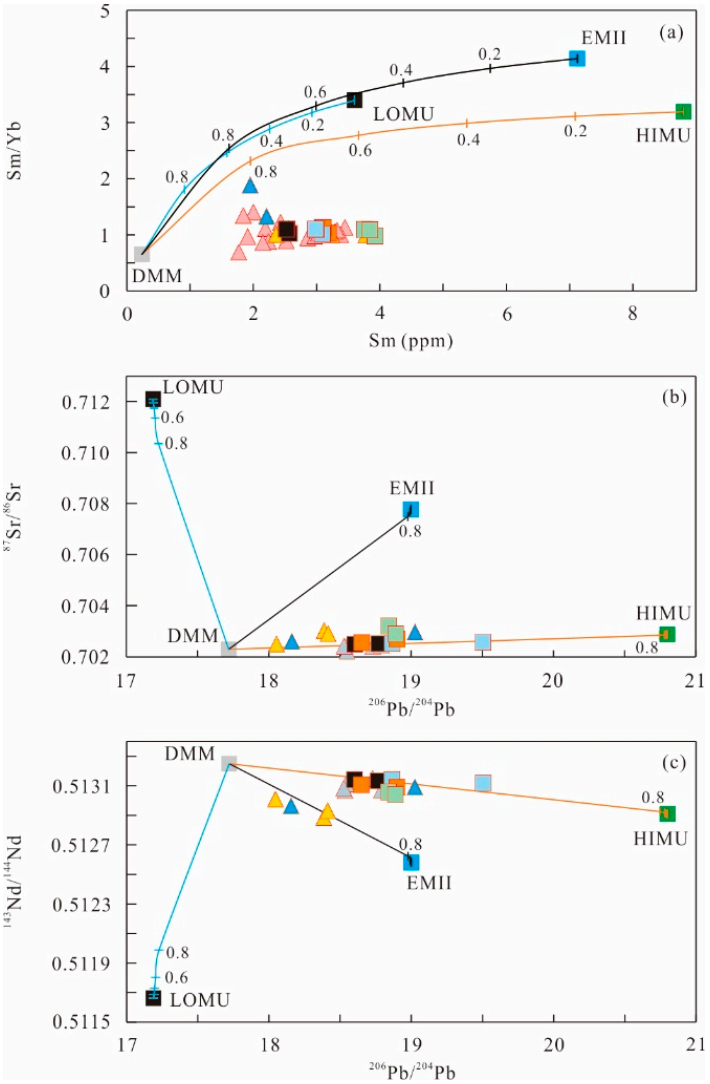

Figure 8. Diagrams of Sm versus Sm/Yb (**a**), $^{206}Pb/^{204}Pb$ versus $^{87}Sr/^{86}Sr$ (**b**), and $^{206}Pb/^{204}Pb$ versus $^{143}Nd/^{144}Nd$ (**c**). The calculated binary mixing lines are shown between the DM, HIMU, EMII, and a LOMU component. The endmember compositions used are shown in Table 3. The numbers on the mixing lines indicate the percentage contribution of the DM components. Symbols are the same as in Figure 2.

5.3. Geodynamic Model

As a mantle plume ascends into the asthenosphere, the ambient subridge mantle upwelling allows the plume components to flow laterally below the lithosphere and melt due to decompression, and the distance of this lateral flow can exceed thousands of kilometers [76]. The geochemical similarities between MORBs and proximal mantle plumes provide evidence that rising components derived from the latter are dynamically entrained and dispersed into the asthenosphere mantle and facilitate the MOR accretion process [15,20,22]. A plume–ridge interaction hypothesis was proposed assuming that regular spatial gradations of Sr–Nd–Pb isotopes in basalts along the MOR axis are associated with mixtures comprising different proportions of a mantle plume and ambient asthenosphere [5,15]. The plume–ridge interaction can account for geochemical and geophysical anomalies along 15–20% of the global MOR system [77].

Table 3. Trace element (ppm) and isotope compositions of mixing model components.

Sample	DMM	HIMU	EMII	LOMU
Sr	7.664	508.95	543.1	143
Nd	0.581	47.18	33.66	9.0
Pb	0.018	3.92	3.92	0.91
Sm	0.239	8.798	7.12	3.6
Yb	0.365	2.757	1.72	1.06
$^{s87}Sr/^{86}Sr$	0.70230	0.70288	0.7078	0.71209
$^{143}Nd/^{144}Nd$	0.513250	0.51291	0.51258	0.511663
$^{206}Pb/^{204}Pb$	17.72	20.8	19.00	17.188

Note: The DMM data is from [26,78]; the HIMU (St. Helena alkali basalts) is from [11] (isotope) and [26] (trace element, N = 32); the EMII data is from [79] (trace element; Tahaa, Society Islands, alkali basalt sample 73-190, recommended by [80]) and [81] (isotope); the LOMU (Glass S18-60/1) data is from [37].

Plumes can affect broad regions of oceanic plates, especially slow-spreading plates [82]. The Atlantic Ocean is a slow-spreading plate where hotspot signatures are identified at ridges as far as 1400 km away from plume sources [82]. The extents of geochemical anomalies in MORBs provide intuitive indicators of the nature and scale of plume–ridge interactions [83]. Previous studies have shown that regional variations in Sr–Nd–Pb–He isotopic ratios in the SMAR MORBs at 12–24°S are due to the broad radial dispersion of materials derived from the St. Helena plume into the asthenosphere (e.g., [6,9,20,22]). At one time, the off-ridge St. Helena plume intersected with the SMAR spreading axis [15]. As a good marker of the deformation process and mantle flow pattern, seismic anisotropy reveals that the plume–ridge interaction below the lithosphere can occur over distances larger than 1000 km through sublithospheric channels [84]. For example, based on the results of seismic tomography (a low-velocity anomaly), Villagomez et al. proposed a connection between the Galápagos plume in the eastern Pacific Ocean and the nearby MOR [85]. In the South Atlantic, seismic tomographic data (combining accurate wavefield computations with the information contained in whole seismic waveforms) indicate that the St. Helena plume spread above the 1000 km horizon at a depth shallower than 250 km with the western mantle flow toward the SMAR [86]. According to high-resolution seismic tomography, other researchers proposed that an inclined sublithospheric channel (slow-spreading zone) likely developed at a shallow depth (~200 km) in the upper mantle that connects the nearby St. Helena plume zone to the westward migrating SMAR [15,27,87]. Coincidentally, the latest waveform tomography results combined with the volcanic ages of the St. Helena Chain and the Cameroon Volcanic Line (CVL, which is a series of oceanic seamounts and continental intrusive centers; Figure 1a) confirm the presence of a continuous and strong low-velocity anomaly between the St. Helena Chain–CVL and the SMAR ([88] and references therein). A lithospheric corridor could exist that allows for the hot asthenosphere to flow from the St. Helena Chain–CVL to the MAR following the gradient of the oceanic lithosphere–asthenosphere boundary [88]. Therefore, a mantle plume–ridge interaction model reflecting dominantly binary mixing between the depleted asthenosphere and the St. Helena hotspot sources probably played an important role in the genesis of the nearby SMAR MORBs.

Although geophysical and geochemical studies indicate that plume–ridge separation distances can exceed 1000 km [89], the ascending off-axis plume effects did not cover all the MOR segments, and the ridge segments without plume effects did not yield any abnormalities in trace element or isotopic compositions [90]. One of the important parameters of the plume–ridge interaction is the distance (D) between them, where the plume effects are the highest at on-axis hotspots and decrease with an increasing plume–ridge separation distance, as indicated by the large variable geochemical signatures of related lavas [91]. For example, a plume–ridge interaction exists between the Pacific–Antarctic Ridge (PAR) and the Foundation hotspot [92]. Geochemical studies indicate that basalts (volcanic cones) that developed between the PAR and the Foundation Seamounts yield E-MORB-like and transitional MORB-like (T-MORB) features, but the amount of basalt alkalinity decreases toward the PAR axis (more T-MORB) [93]. In addition, Yang et al. found that isotopically-enriched N-MORBs

occurred on the Southwest Indian Ridge (SWIR) at 50°28′E [94]. These rocks were produced with the involvement of Crozet plume components, and the enriched materials may have experienced decompression melting (low-degree) to become depleted in incompatible elements, but their isotopic compositions did not obviously change during the upslope flow of the Crozet plume to the ridge [94]. Notably, isotopically enriched N-MORBs mainly occur at slower-spreading ridges with a large plume–ridge distance (~1000 km) [94]. Nevertheless, the changes in the trace element and isotopic compositions of MORBs mostly depend on the geochemical diversity in their mantle source regions [90]. It is usually accepted that plumes can flow along and toward MORs in a pancake- or pipe-like channel [77]. For example, some off-axis plumes located at appreciable distances, including the Easter-Salas y Gomez and Galápagos plumes, are considered to interact with their nearby MORs through pipeline-like flows (channels) along the base of the lithosphere [95]. The plume effect differs between a "pipe-like channel" plume and a "pancake-like channel" plume. An off-ridge plume with a "pancake-like channel" can affect the ambient mantle nondirectionally, but the range of influence of an off-ridge plume with a pipe-like channel is selective and can be limited or even insignificant when considering the impact of the channel direction [90].

The MORBs from the SMAR at 18–21°S were located near St. Helena island (~800 km; Figure 1b). The discussion in Section 5.2 revealed their likely origin from a DM source with the involvement of minor St. Helena hotspot components and minor EMII-type components that came from recycled metasomatized oceanic crust. This inference indicates that the asthenosphere beneath the SMAR at 18–21°S was likely contaminated by the St. Helena plume. Moreover, the MORBs from the SMAR at 18–21°S showed E-MORB- to N-MORB-like geochemical characteristics (dominated by N-MORB-like rocks; Figure 6) with different Sr–Nd–Pb isotopic compositions extending from depleted to enriched endmembers (Figures 2–5). According to the discussions above, we ascribed these geochemical phenomena to the shape of the plume flow toward the SMAR insomuch as the SMAR MORBs at 18–21°S may have been formed through pipe-like channels. This means that the HIMU-type materials derived from the St. Helena hotspot and injected into the depleted asthenosphere beneath the axial SMAR at 18–21°S were possibly transported through so-called pipe-like inclined sublithospheric channels into the SMAR axial zone. Namely, the SMAR MORBs at 18–21°S may have formed from a plume–ridge interaction model with pipeline-like plume flows along the base of the lithosphere toward the SMAR but with different proportions of components (referring mainly to DM and St. Helena HIMU-type plume components) in their source regions.

Previous studies have shown that recycled subducted oceanic crust can be entrained in upwelling mantle plumes [26,96,97]. As mentioned above, HIMU is a mantle reservoir that is considered to have been formed by subduction and the subsequent storage of an ancient oceanic crust and lithosphere in the mantle (e.g., [54,64]). Kawabata et al. proposed that the primary magmas of the St. Helena plume may have originated from the partial melting of a DM source with the addition of a small melt quantity that was derived from recycled ancient subducted oceanic crust [26]. The calculation for the recycled crust involved in the genesis of St. Helena basalts yields $^{87}Sr/^{86}Sr$ = 0.7017–0.7042 and $^{206}Pb/^{204}Pb$ = 21.7–73.9 [26]. These ratios are different from those ($^{87}Sr/^{86}Sr$ > 0.707 and $^{206}Pb/^{204}Pb$ = 18.5–19.5) of the EMII endmember reported by [42,81]. This means that the minor involved EMII-type components that originated from recycled metasomatized oceanic crust in the genesis of the SMAR MORBs at 18–21°S may not have been derived from the St. Helena plume. The contribution of recycled metasomatized oceanic crust components (EMII-type materials) to the formation of the SMAR MORBs at 18–21°S was possibly related to the early dispersion of other plume heads into the subcontinental asthenosphere prior to the opening of the South Atlantic Ocean [6,20], where they were then sampled by MORB-related magmatism, which is represented by the SMAR MORBs at 18–21°S.

6. Conclusions

The isotope compositions of the SMAR MORBs at 18–21°S indicate that these rocks originated from a heterogeneous mantle substrate related to a mixture of DM components (>80%) with a small but

variable amount of HIMU- and EMII-type components. The HIMU-type components likely originated from the adjacent St. Helena hotspot. The SMAR MORBs at 18–21°S were potentially formed by plume–ridge interactions with pipeline-like mantle flows that were derived from the St. Helena plume along the base of the lithosphere toward the SMAR. The EMII-type components may have been derived from recycled metasomatized oceanic crust and possibly originated from the early dispersion of other plume heads into the subcontinental asthenosphere prior to the opening of the South Atlantic Ocean. In addition, the contributions from subducted sediments, continental crust, and subcontinental lithospheric mantle materials to the genesis of the SMAR MORBs at 18–21°S may have been nonexistent or negligible.

Supplementary Materials: The following are available online at http://www.mdpi.com/2075-163X/10/11/1010/s1, Table S1. Sr, Nd, Pb and Hf isotope ratios in geochemical reference materials of USGS.

Author Contributions: Conceptualization, W.L.(Weiliang Liu), Y.Z. and Y.G.; methodology, W.L.(Weiliang Liu) and Y.Z.; validation, W.L.(Weiliang Liu) and Y.Z.; formal analysis, X.Z.; investigation, Z.S.; resources, Z.S.; data curation, X.Z.; writing—original draft preparation, Y.Z.; writing—review and editing, W.L.(Weiliang Liu) and Y.Z.; visualization, J.L., W.L.(Wei Li), Y.M. and Y.G.; supervision, W.L.(Weiliang Liu); project administration, B.X.; funding acquisition, W.L.(Weiliang Liu). All authors have read and agreed to the published version of the manuscript.

Funding: This work was supported by the National Nature Science Foundation of China (grant numbers 41972049, 41472054, 41373012); Guangzhou Science Technology and Innovation Commission Project (grant number 201904010138); a research grant from the State Key Laboratory of Isotope Geochemistry, Guangzhou Institute of Geochemistry, Chinese Academy of Sciences (grant number SKLaBIG–KF–18–11); China State Scholarship Fund of visiting scholar (grant number 20170638507); the Special Fund for Basic Scientific Research of Central Colleges, Chang'an University (grant numbers 300102269504, 300102268502, 300102260502); National Higher Education Quality Monitoring Data Center of Sun Yat-sen University (grant number G1914) and SYSU Course Construction Project for Postgraduates (grant number 201922).

Acknowledgments: We thank teamwork of crews on the China's 26th ocean expedition and marine geologic survey training supported by the South China Sea cruises, South China Sea Institute, SYSU. We are deeply grateful to Ye Lu for the quantitative modeling and Chris Yakymchuk for the English editing. We appreciate two anonymous reviewers for their constructive comments and suggestions.

Conflicts of Interest: The authors declare no conflict of interest.

References

1. Wilkinson, J.F.G. The genesis of Mid–Ocean ridge basalt. *Earth Sci. Rev.* **1982**, *18*, 1–57. [CrossRef]
2. Le Roux, P.J.; le Roex, A.L.; Schilling, J.G. Crystallization processes beneath the southern Mid–Atlantic Ridge (40–55° S), evidence for high–pressure initiation of crystallization. *Contrib. Mineral. Petrol.* **2002**, *142*, 582–602. [CrossRef]
3. Sun, S.S.; Nesbit, R.W.; Sharaskin, A. Chemical characteristics of mid–ocean ridge basalts. *Earth Planet. Sci. Lett.* **1979**, *45*, 119–138. [CrossRef]
4. Wood, D.A.; Joron, J.L.; Treuil, M.; Norry, M.; Tarney, J. Elemental and Sr isotope variations in basic lavas from Iceland and the surrounding ocean floor. *Contrib. Mineral. Petrol.* **1979**, *70*, 319–339. [CrossRef]
5. Schilling, J.G. Upper mantle heterogeneities and dynamics. *Nature* **1985**, *314*, 62–67. [CrossRef]
6. Graham, D.W.; Jenkins, W.J.; Schilling, J.G.; Thompson, G.; Kurz, M.D.; Humphris, S.E. Helium isotope geochemistry of mid–ocean ridge basalts from the South Atlantic. *Earth Planet. Sci. Lett.* **1992**, *110*, 133–147. [CrossRef]
7. Andres, M.; Blichert–Toft, J.; Schilling, J.G. Hafnium isotopes in basalts from the southern Mid–Atlantic Ridge from 40° S to 55° S: Discovery and Shona plume–ridge interactions and the role of recycled sediments. *Geochem. Geophys. Geosyst.* **2002**, *3*, 1–25. [CrossRef]
8. Hoernle, K.; Hauff, F.; Kokfelt, T.F.; Haase, K.; Garbe–Schonberg, D.; Werner, R. On– and off–axis chemical heterogeneities along the South Atlantic Mid–Ocean–Ridge (5–11° S): Shallow or deep recycling of ocean crust and/or intraplate volcanism? *Earth Planet. Sci. Lett.* **2011**, *306*, 86–97. [CrossRef]
9. Skolotnev, S.G.; Peive, A.A.; Belyatskii, B.V. Geochemical and isotopic features of basalts in the axial Mid–Atlantic Ridge near the Martin Vaz Fracture Zone, South Atlantic (19°–20° S). *Dokl. Earth Sci.* **2006**, *407*, 401–407. [CrossRef]

10. Turner, S.; Kokfelt, T.; Hauff, F.; Hasse, K.; Lundstrom, C.; Hoernle, K.; Yeo, I.; Devey, C. Mid–ocean ridge basalt generation along the slow–spreading, South Mid–Atlantic Ridge (5–11° S): Inferences from ^{238}U–^{230}Th–^{226}Ra disequilibria. *Geochim. Cosmochim. Acta.* **2015**, *169*, 152–166. [CrossRef]
11. Douglass, J.; Schilling, J.G. Systematics of three–component, pseudo–binary mixing lines in 2D isotope ratio space representations and implications for mantle plume–ridge interaction. *Chem. Geol.* **2000**, *163*, 1–23. [CrossRef]
12. Zindler, A.H.; Staudigel, H.; Batiza, R. Isotope and trace element geochemistry of young Pacific seamounts: Implications for the scale of upper mantle heterogeneity. *Earth Planet. Sci. Lett.* **1984**, *70*, 175–195. [CrossRef]
13. Gurnis, M. Quantitative bounds on the size spectrum of isotopic heterogeneity within the mantle. *Nature* **1986**, *323*, 317–320. [CrossRef]
14. Graham, D.W.; Zindler, A.; Kurz, M.D.; Jenkins, W.J.; Batiza, R.; Staudigel, H. He, Pb, Sr and Nd isotope constraints on magma genesis and mantle heterogeneity beneath young Pacific seamounts. *Contrib. Miner. Petrol.* **1988**, *99*, 446–463. [CrossRef]
15. Schilling, J.G.; Thompson, G.; Kingsley, R.; Humphris, S. Hotspot–migrating ridge interaction in the South Atlantic. *Nature* **1985**, *313*, 187–191. [CrossRef]
16. Douglass, J.; Schilling, J.G.; Fontignie, D. Plume–ridge interactions of the Discovery and Shona mantle plumes with the southern Mid–Atlantic Ridge (40°–55° S). *J. Geophys. Res. Solid Earth* **1999**, *104*, 2941–2962. [CrossRef]
17. Vlastélic, I.; Dosso, L. Initiation of a plume–ridge interaction in the South Pacific recorded by high–precision Pb isotopes along Hollister Ridge. *Geochem. Geophys. Geosyst.* **2005**, *6*, 1–13. [CrossRef]
18. Singh, S.C.; Carton, H.; Chauhan, A.S.; Androvandi, S.; Davaille, A.; Dyment, J.; Cannat, M.; Hananto, N.D. Extremely thin crust in the Indian ocean possibly resulting from plume–ridge interaction. *Geophys. J. Int.* **2011**, *1*, 29–42. [CrossRef]
19. Herbrich, A.; Hauff, F.; Hoernle, K.; Werner, R.; Garbe–Schonberg, D.; White, S. A 1.5 Ma record of plume–ridge interaction at the Western Galápagos Spreading Center (91°40′–92°00′ W). *Geochim. Cosmochim. Acta.* **2016**, *185*, 141–159. [CrossRef]
20. Fontignie, D.; Schilling, J.G. Mantle heterogeneities beneath the South Atlantic: A Nd–Sr–Pb isotope study along the Mid–Atlantic Ridge (3° S–46° S). *Earth Planet. Sci. Lett.* **1996**, *142*, 209–221. [CrossRef]
21. Ding, X.; Li, J.; Zheng, C.Q.; Huang, W.; Cui, N.Y.; Dou, Y.G.; Sun, Z.L. Chemical composition of the basalts on East Pacific rise (1.5° N~1.5° S) and South Mid–Atlantic ridge (13.2° S). *Marin. Geol. Quat. Geol.* **2014**, *34*, 57–66. [CrossRef]
22. Hanan, B.B.; Kingsley, R.H.; Schilling, J. Pb isotope evidence in the South Atlantic for migrating ridge–hotspot interactions. *Nature* **1986**, *322*, 137–144. [CrossRef]
23. Qi, Q.; Lai, Z.Q.; Long, X.J.; Leng, C.X.; Zhao, G.T. Characteristics and Petrogenesis Significance of Plagioclases in Basalt from the South Mid–Atlantic Ridge. *Perio. China Univ. Ocean.* **2016**, *46*, 105–112, (In Chinese with English abstract). [CrossRef]
24. Stakes, D.S.; Shervais, J.W.; Hopson, C.A. The volcanic–tectonic cycle of the FAMOUS and AMAR Valleys, Mid–Atlantic Ridge (36°47′ N): Evidence from basalt glass and phenocryst compositional variations for a steady state magma chamber beneath the valley midsections, AMAR 3. *J. Geophys. Res. Solid Earth* **1984**, *89*, 6995–7028. [CrossRef]
25. Smith, W.H.F.; Sandwell, D.T. Global seafloor topography from satellite altimetry and ship depth soundings. *Science* **1997**, *277*, 1957–1962. [CrossRef]
26. Kawabata, H.; Hanyu, T.; Chang, Q.; Kimura, J.I.; Nichols, A.R.L.; Tatsumi, Y. The petrology and geochemistry of St. Helena alkali basalts: Evaluation of the oceanic crust–recycling model for HIMU OIB. *J. Petrol.* **2011**, *52*, 791–838. [CrossRef]
27. Zhang, Y.S.; Tanimoto, T. Ridges, hotspots and their interaction as observed in seismic velocity maps. *Nature* **1992**, *355*, 45–49. [CrossRef]
28. Zhang, H.T. Mid–Oceanic Ridge Basalts (MORBS) Chemistry and Characteristics of Plagioclase–Hosted Melt Inclusions in the South Atlantic Ridge 19° S and Implications for Magmatic Processes. Master's Thesis, First Institute of Oceanography SOA, Qingdao, China, 2015.
29. Douglass, J.; Schilling, J.; Fontignie, D. The Discovery and Shona mantle plumes and the LO–MU component: An inexorable connection. In Proceedings of the AGU Fall Meeting, San Francisco, CA, USA, 15–19 December 1996.

30. Zhong, Y.; Liu, W.L.; Sun, Z.L.; Yakymchuk, C.; Ren, F.F.; Liu, J.N.; Li, W.; Ma, Y.L.; Xia, B. Geochemistry and Mineralogy of Basalts from the South Mid–Atlantic Ridge (18.0°–20.6° S): Evidence of a Heterogeneous Mantle Source. *Minerals* **2019**, *9*, 659. [CrossRef]
31. Qi, Q. Petrogeochemical Characteristics Comparison and Implication for Magmatic Processes of the MORBs between SAR and SWIR. Master's Thesis, Ocean University of China, Qingdao, China, 2015.
32. Encyclopædia Britannica. Mid-Atlantic Ridge. 2020. Available online: https://www.britannica.com/place/Mid-Atlantic-Ridge (accessed on 8 August 2018).
33. Murton, B.J.; Rona, P.A. Carlsberg ridge and Mid–Atlantic ridge: Comparison of slow spreading Centre analogues. *Deep Sea Res. Part II* **2015**, *121*, 71–84. [CrossRef]
34. Xu, W.; Guo, S.S.; Pang, K.L.; Luo, Z.H. Fungi associated with chimney and sulfide samples from a South Mid–Atlantic Ridge hydrothermal site: Distribution, diversity and abundance. *Deep Sea Res. Part. I* **2017**, *123*, 48–55. [CrossRef]
35. Moreira, M.; Staudacher, T.; Sarda, P.; Schilling, J.G.; Allégre, C.J. A primitive plume neon component in MORB: The Shona–Ridge anomaly, South Atlantic (51–52° S). *Earth Planet. Sci. Lett.* **1995**, *133*, 367–377. [CrossRef]
36. Sarda, P.; Moreira, M.; Staudacher, T.; Schilling, J.G.; Allégre, C.J. Rare gas systematics on the southernmost Mid–Atlantic Ridge: Constraints on the lower mantle and the Dupal source. *J. Geophys. Res. Solid Earth* **2000**, *105*, 5973–5996. [CrossRef]
37. Kamenetsky, V.S.; Maas, R.; Sushchevskaya, N.M.; Norman, M.D.; Cartwright, I.; Peyve, A.A. Remnants of Gondwanan continental lithosphere in oceanic upper mantle: Evidence from the South Atlantic Ridge. *Geology* **2001**, *29*, 243. [CrossRef]
38. Cande, S.C.; Kent, D.V. A new geomagnetic polarity time scale for the Late Cretaceous and Cenozoic. *J. Geophys. Res. Solid Earth* **1992**, *97*, 13917–13951. [CrossRef]
39. Kawabata, H.; Hanyu, T. Magmatic processes for producing the variations from ankaramites to phenocryst–poor basalts: An example from St. Helena Island. In Proceedings of the AGU Fall Meeting, San Francisco, CA, USA, 5–8 December 2005.
40. Morgan, W.J. Convection plumes on the lower mantle. *Nature* **1971**, *230*, 42–43. [CrossRef]
41. Emery, K.O.; Uchupi, E. The Geology of the Atlantic Ocean. *Geol. Foeren. Stockholm Foerh.* **1984**, *108*, 197–198. [CrossRef]
42. Zindler, A.; Hart, S. Chemical geodynamics. *Annu. Rev. Earth Planet. Sci.* **1986**, *14*, 493–571. [CrossRef]
43. Weis, D.; Kieffer, B.; Maerschalk, C.; Barling, J.; De Jong, J.; Williams, G.A.; Hanano, D.; Pretorius, W.; Mattielli, N.; Scoates, J.; et al. High–precision isotopic characterization of USGS reference materials by TIMS and MC–ICP–MS. *Geochem. Geophys. Geosyst.* **2006**, *7*, 139–149. [CrossRef]
44. Weis, D.; Kieffer, B.; Hanano, D.; Silva, I.N.; Barling, J.; Pretorius, W.; Maerschalk, C.; Mattielli, N. Hf isotope compositions of U.S. Geological Survey reference materials. *Geochem. Geophys. Geosyst.* **2007**, *8*, 1–15. [CrossRef]
45. Hart, S.R. A large–scale isotope anomaly in the Southern Hemisphere mantle. *Nature* **1984**, *309*, 753–757. [CrossRef]
46. Hart, S.R. Heterogeneous mantle domains: Signatures, genesis and mixing chronologies. *Earth Planet. Sci. Lett.* **1988**, *90*, 273–296. [CrossRef]
47. Choi, S.H.; Mukasa, S.B.; Kwon, S.T.; Andronikov, A.V. Sr, Nd, Pb and Hf isotopic compositions of late Cenozoic alkali basalts in South Korea: Evidence for mixing between the two dominant asthenospheric mantle domains beneath East Asia. *Chem. Geol.* **2006**, *232*, 134–151. [CrossRef]
48. Sun, S.S. Lead isotopic study of young volcanic rocks from mid–ocean ridges, ocean islands and island arcs. *Phil. Trans. R. Soc. Lond.* **1980**, *A297*, 409–445. [CrossRef]
49. Hoernle, K.A.; Tilton, G.R. Sr–Nd–Pb isotope data for Fuerteventura (Canary Islands) basal complex and subaerial volcanics: Applications to magma genesis and evolution. *Schweiz. Mineral. Petrogr. Mitt.* **1991**, *71*, 3–18. [CrossRef]
50. Hoernle, K.A.J. Geochemistry of Jurassic oceanic crust beneath Gran Canaria (Canary Islands): Implications for crustal recycling and assimilation. *J. Petrol.* **1998**, *39*, 859–880. [CrossRef]
51. Rehkamper, M.; Hofmann, A.W. Recycled ocean crust and sediment in Indian Ocean MORB. *Earth Planet. Sci. Lett.* **1997**, *147*, 93–106. [CrossRef]
52. Plank, T.; Langmuir, C.H. The chemical composition of subducting sediment and its consequences for the crust and mantle. *Chem. Geol.* **1998**, *145*, 325–394. [CrossRef]
53. Rollinson, H. *Using Geochemical Data: Evaluation, Presentation, Interpretation*; Longman Scientific and Technical: London, UK, 1993; p. 240. ISBN 0582218632.

54. Salters, V.J.M.; White, W.M. Hf isotope constraints on mantle evolution. *Chem. Geol.* **1998**, *145*, 447–460. [CrossRef]
55. Gale, A.; Dalton, C.A.; Langmuir, C.H. The mean composition of ocean ridge basalts. *Geochem. Geophys. Geosyst.* **2013**, *14*, 489–518. [CrossRef]
56. Kamenetsky, V.S.; Everard, J.L.; Crawford, A.J.; Varne, R.; Eggins, S.M.; Lanyon, A.R. Enriched End-member of Primitive MORB Melts: Petrology and Geochemistry of Glasses from Macquarie Island (SW Pacific). *J. Petrol.* **2000**, *41*, 411–430. [CrossRef]
57. Le Roux, P.J.; le Roex, A.L.; Schilling, J.G.; Shimizu, N.; Perkins, W.W.; Pearce, N.J.G. Mantle heterogeneity beneath the Southern Mid–Atlantic Ridge: Trace element evidence for contamination of ambient asthenosphere mantle. *Earth Planet. Sci. Lett.* **2002**, *203*, 479–499. [CrossRef]
58. Sun, S.S.; McDonough, W.F. Chemical and isotopic systematics of oceanic basalt: Implication for mantle composition and processes. *Geol. Soc. Lond. Spec. Publ.* **1989**, *42*, 528–548. [CrossRef]
59. Tatsumoto, M.; Nakamura, Y. DUPAL anomaly in the Sea of Japan: Pb, Nd, and Sr isotopic variations at the eastern Eurasian continental margin. *Geochem. Cosmochem. Acta* **1991**, *55*, 3697–3708. [CrossRef]
60. Weaver, B.L. Trace element evidence for the origin of ocean–island basalts. *Geology* **1991**, *19*, 123–126. [CrossRef]
61. Chauvel, C.; Hofmann, A.W.; Vidal, P. HIMU–EM: The French Polynesian connection. *Earth Planet. Sci. Lett.* **1992**, *110*, 99–119. [CrossRef]
62. Hauri, E.H.; Shimizu, N.; Dieu, J.J.; Hart, S.R. Evidence for hotspot–related carbonatite metasomatism in the oceanic upper mantle. *Nature* **1993**, *365*, 221–227. [CrossRef]
63. Willbold, M.; Stracke, A. Upper and lower continental crust in the sources of ocean island basalts—isotopic and chemical constraints. *Geochim. Cosmochim. Acta* **2006**, *70*, A702. [CrossRef]
64. Chauvel, C.; Lewin, E.; Carpentier, M.; Arndt, N.T.; Marini, J.C. Role of recycled oceanic basalt and sediment in generating the Hf–Nd mantle array. *Nat. Geosci.* **2008**, *1*, 64–67. [CrossRef]
65. Thompson, R.N.; Morrison, M.A.; Hendry, G.L.; Parry, S.J. An Assessment of the Relative Roles of Crust and Mantle in Magma Genesis: An Elemental Approach. *Philos. Trans. R. Soc. A Math. Phys. Sci.* **1984**, *310*, 549–590. [CrossRef]
66. Alibert, C. Mineralogy and geochemistry of a basalt from Site 738: Implications for the tectonic history of the southernmost part of the Kerguelen Plateau. In *Proceedings of the Ocean Drilling Program, Scientific Results*; Barron, J., Larsen, B., Eds.; Publications Distribution Center: Texas, TX, USA, 1991; Volume 119, pp. 293–297. ISBN 978-000-884-588-9.
67. Mahoney, J.J.; Jones, W.B.; Frey, F.A.; Salters, V.J.M.; Pyle, D.G.; Davies, H.L. Geochemical characteristics of lavas from Broken Ridge, the Naturaliste Plateau and southernmost Kerguelen Plateau: Cretaceous plateau volcanism in the southeast Indian Ocean. *Chem. Geol.* **1995**, *120*, 315–345. [CrossRef]
68. Frey, F.A.; Mcnaughton, N.J.; Nelson, D.R.; de Laeter, J.R.; Duncan, R.A. Petrogenesis of the Bunbury Basalt, Western Australia: Interaction between the Kerguelen plume and Gondwana lithosphere? *J. Afr. Earth Sci.* **1996**, *26*, 519–522. [CrossRef]
69. Rudnick, R.; Gao, S. The role of lower crustal recycling in continent formation. *Geochim. Cosmochim. Acta* **2003**, *67*, 1–10.
70. Zhao, J.H.; Zhou, M.F. Geochemistry of Neoproterozoic mafic intrusions in the Panzhihua district (Sichuan Province, SW China): Implications for subduction related metasomatism in the upper mantle. *Precambrian Res.* **2007**, *152*, 27–47. [CrossRef]
71. Plank, T. Constraints from thorium/lanthanum on sediment recycling at subduction zones and the evolution of the continents. *J. Petrol.* **2005**, *46*, 921–944. [CrossRef]
72. Taylor, S.R.; Mclennan, S.M. The geochemical evolution of the continental crust. *Rev. Geophys.* **1995**, *33*, 241–265. [CrossRef]
73. Mahoney, J.; LeRoex, A.P.; Peng, Z.; Fisher, R.L.; Natland, J.H. Southwestern limits of Indian Ocean Ridge mantle and the origin of low $^{206}Pb/^{204}Pb$ mid–ocean ridge basalt: Isotope systematics of the central southwest Indian Ridge (17°–50° E). *J. Geophys. Res. Solid Earth* **1992**, *97*, 19771–19790. [CrossRef]
74. Fitton, J.G. The OIB paradox. *Spec. Pap. Geol. Soc. Am.* **2007**, *430*, 387–412. [CrossRef]
75. Weaver, B. St. Helena Revisited: Characteristics and Origin of the Type HIMU OIB. In Proceedings of the AGU Fall Meeting, San Francisco, CA, USA, 11–15 December 2006.
76. Niu, Y.L.; Collerson, K.D.; Batiza, R. Origin of enriched–type mid–ocean ridge basalt at ridges far from mantle plumes: The East Pacific Rise at 11°20′ N. *J. Geophys. Res. Solid Earth* **1999**, *104*, 7076–7087. [CrossRef]

77. Ito, G.; Lin, J.; Graham, D. Observational and theoretical studies of the dynamics of mantle plume–mid-ocean ridge interaction. *Rev. Geophys.* **2003**, *41*, 1–24. [CrossRef]
78. Su, Y. Global MORB Chemistry Compilation at the Segment Scale. Ph.D. Thesis, Columbia University, New York, NY, USA, 2003.
79. White, W.M.; Duncan, R.A. Geochemistry and geochronology of the Society Islands: New evidence for deep mantle recycling. *Geophys. Monogr.* **1996**, *95*, 1–23. [CrossRef]
80. Hofmann, A.W. Sampling mantle heterogeneity through oceanic basalts: Isotopes and trace elements. *Treatise Geochem.* **2004**, *2*, 1–44. [CrossRef]
81. Hart, S.R.; Hauri, E.H.; Oschmann, L.A.; Whitehead, J.A. Mantle plumes and entrainment: Isotopic evidence. *Science* **1992**, *256*, 517–520. [CrossRef] [PubMed]
82. Ito, G.; Lin, J.; Gable, C.W. Interaction of mantle plumes and migrating mid–ocean ridges: Implications for the Galapagos plume–ridge system. *J. Geophys. Res.* **1997**, *102*, 15403–15417. [CrossRef]
83. Bourdon, B.; Langmuir, C.H.; Zindler, A. Ridge–hotspot interaction along the Mid–Atlantic Ridge between 37°30′ and 40°30′ N: The U–Th disequilibrium evidence. *Earth Planet. Sci. Lett.* **1996**, *142*, 175–189. [CrossRef]
84. Montagner, J.P.; Stutzmann, E.; Sicilia, D.; Sebai, A.; Beucler, E.; Silveira, G.; Cara, M.; Debayle, E.; Leveque, J.J. Plume-Ridge Lithospheric Interactions: Cases of Afar (Africa). In Proceedings of the EGS—AGU—EUG Joint Assembly Meeting, Nice, France, 6–11 April 2003.
85. Villagomez, D.R.; Toomey, D.R.; Geist, D.J.; Hooft, E.E.E.; Solomon, S.C. Mantle flow and multistage melting beneath the Galapagos hotspot revealed by seismic imaging. *Nat. Geosci.* **2014**, *7*, 151–156. [CrossRef]
86. French, S.W.; Bomanowicz, B. Broad plumes rooted at the base of the Earth's mantle beneath major hotspots. *Nature* **2015**, *525*, 95–113. [CrossRef]
87. Zhang, Y.S.; Tanimoto, T.; Stolper, E.M. S–wave velocity, basalt chemistry and bathymetry along the Mid–Atlantic Ridge. *Phys. Earth Planet. Inter.* **1994**, *84*, 79–93. [CrossRef]
88. Celli, N.L.; Lebedev, S.; Schaeffer, A.J.; Ravenna, M.; Gaina, C. The upper mantle beneath the South Atlantic Ocean, South America and Africa from waveform tomography with massive data sets. *Geophys. J. Int.* **2020**, *221*, 178–204. [CrossRef]
89. Ribe, N.M. The dynamics of plume–ridge interaction, 2, Off–ridge plumes. *J. Geophys. Res.* **1996**, *101*, 16195–16204. [CrossRef]
90. Guan, Y.L.; Shi, X.F.; Yan, Q.S.; Wei, X.; Zhang, Y.; Xia, X.P.; Zhou, H.D. Implications of the melting depth and temperature of the Atlantic mid–ocean ridge basalts. *Acta Oceanol. Sin.* **2019**, *38*, 35–42. [CrossRef]
91. Ito, G.; Lin, J. Oceanic spreading center–hotspot interactions: Constraints from along–isochron bathymetric and gravity anomalies. *Geology* **1995**, *23*, 657–660. [CrossRef]
92. Maia, M.; Ackermand, D.; Dehghani, G.A.; Gente, P.; Hekinian, R.; Naar, D.; Connor, J.O.; Perrot, K.; Morgan, J.P.; Ramillien, G.; et al. The Pacific–Antarctic Ridge–Foundation hotspot interaction: A case study of a ridge approaching a hotspot. *Mar. Geol.* **2000**, *167*, 61–84. [CrossRef]
93. Hekinian, R.; Stoffers, P.; Ackermand, D.; Réveillon, S.; Maia, M.; Bohn, M. Ridge–hotspot interaction: The Pacific–Antarctic Ridge and the foundation seamounts. *Mar. Geol.* **1999**, *160*, 199–223. [CrossRef]
94. Yang, A.Y.; Zhao, T.P.; Zhou, M.F.; Deng, X.G. Isotopically enriched N-MORB: A new geochemical signature of off–axis plume–ridge interaction—A case study at 50°28′ E, Southwest Indian Ridge. *J. Geophys. Res. Solid Earth* **2017**, *122*, 191–213. [CrossRef]
95. Morgan, W.J. Rodriguez, Darwin, Amsterdam, . . . , a second type of hotspot island. *J. Geophys. Res.* **1978**, *83*, 5355–5360. [CrossRef]
96. Yasuda, A.; Fujii, T. Ascending subducted oceanic crust entrained within mantle plumes. *Geophys. Res. Lett.* **1998**, *25*, 1561–1564. [CrossRef]
97. Li, M.M.; Mcnamara, A.K.; Garnero, E.J. Chemical complexity of hotspots caused by cycling oceanic crust through mantle reservoirs. *Nat. Geosci.* **2014**, *7*, 366–370. [CrossRef]